The Structure, Dynamics, and Origin of a Small-Scale Lens of Water in the Western North Atlantic Thermocline*

STEPHEN C. RISER

School of Oceanography, University of Washington, Seattle, WA 98195

W. BRECHNER OWENS

Woods Hole Oceanographic Institution, Woods Hole, MA 02543

H. THOMAS ROSSBY

Graduate School of Oceanography, University of Rhode Island, Kingston, RI 02881

CURTIS C. EBBESMEYER

Evans-Hamilton, Inc., Seattle, WA 98115

(Manuscript received 28 February 1984, in final form 14 June 1985)

ABSTRACT

A small-scale, isolated, anticyclonically rotating lens of water was observed in the western North Atlantic thermocline during the POLYMODE Local Dynamics Experiment. Using a combination of SOFAR float, hydrographic, nutrient, and moored current and temperature data, we deduce that the lens was about 20 km across, with a thickness not greater than 300 m, centered on 750 m; that its shape was not dissimilar to that of a vertical–radial Gaussian eddy; and that at its center, the lens had strong anomalies of salinity, dissolved oxygen, nitrate, and vortex stretching. The water mass properties within the eddy are not inconsistent with an origin for the feature near 15°N, 54°W, several thousand kilometers from where it was observed in the western North Atlantic, although an unambiguous origin cannot be discerned from the data. If such features are not uncommon, they may be an important mechanism for large-scale mixing of water properties in the ocean.

1. Introduction

The POLYMODE Local Dynamics Experiment (LDE) was a major cooperative program undertaken from May through July 1978, to explore the mesoscale eddy field in an energetic area of the western North Atlantic. Centered on 31°N, 69°30′W, the field observations consisted of measurements of current and temperature from 10 moorings (Owens et al., 1982); numerous conductivity/temperature/pressure/dissolved oxygen (CTD–O_2) casts and expendable bathythermograph (XBT) profiles from several ships (Taft et al., 1985); and trajectories from 40 SOFAR floats (Rossby et al., 1985).

The focus of the experiment was on the interaction of mesoscale eddies, having characteristic length scales of 50–100 km, with the mean field in the region. An unanticipated bonus, however, was the discovery of a class of energetic, small (~20 km across), isolated (both horizontally and vertically), apparently long-lived eddies in the region. These features were structurally similar to the eddy of Mediterranean origin found in the western North Atlantic near 24°N, 70°W by McDowell and Rossby (1978). In general, however, the LDE features were considerably smaller than the Mediterranean eddy and appeared to originate from a number of disparate regions of the North Atlantic basin.

At least 31 distinct eddies of this type were observed during the experiment; their collective properties have been documented by Lindstrom and Taft (1986). In this paper, we report on the structural, kinematic, and dynamic characteristics of one such feature observed in the main thermocline during the experiment. The feature, named "S1" (for shallow feature number 1), rotated anticyclonically, was about 300 m thick centered on the $\sigma_\theta = 27.05$ surface[1] (about 750 m depth), and had a diameter of roughly 20 km. The water in the core of S1 showed strong anomalies of salinity, O_2, nitrate, and vortex stretching, compared to background

* Contribution number 1431 from the School of Oceanography, University of Washington, and Contribution number 5518 of the Woods Hole Oceanographic Institution.

[1] Throughout this paper the units of σ_θ are understood to be 10^{-3} g cm^{-3}.

Sargasso Sea water. Taken together, these anomalous properties allow us to suggest several scenarios for the origin of the feature; each of these scenarios implies that the water comprising S1 originated 1000–2000 km south of the LDE region. The properties of S1 can be compared to those of two other isolated features observed in detail during the experiment that are discussed elsewhere in this issue (Lindstrom and Taft, 1986; Elliott and Sanford, 1986).

2. Observations and hydrographic structure

A large amount of data, from a variety of instruments, was collected from the vicinity of S1. The times and locations of these observations are summarized in Fig. 1. Two SOFAR floats were launched quite by accident near the feature in May 1978 during cruise 21 of R.V. *Endeavor*, at the beginning of the LDE. During the float recovery cruise aboard the R.V. *Gyre* (Cruise 78G6) in July 1978, a number of XBTs were taken near the final float positions, and continuous profiles of salinity, temperature, pressure and O_2 were taken very near the center of S1, using a Plessey Model 9040 CTD with a Beckmann dissolved oxygen sensor. Dissolved silicate and nitrate were measured at the eddy center from Niskin bottles mounted on the rosette sampler on the CTD. In addition to these Lagrangian views of S1, Eulerian information was collected as the feature moved (again, quite by accident) through the LDE moored current/temperature meter array (Owens et al., 1982) and close to the positions of several hydrographic stations taken on the grid used for the LDE density program (Taft et al., 1986). A synthesis of these datasets provides us with considerable information on both the horizontal and vertical structure of the feature.

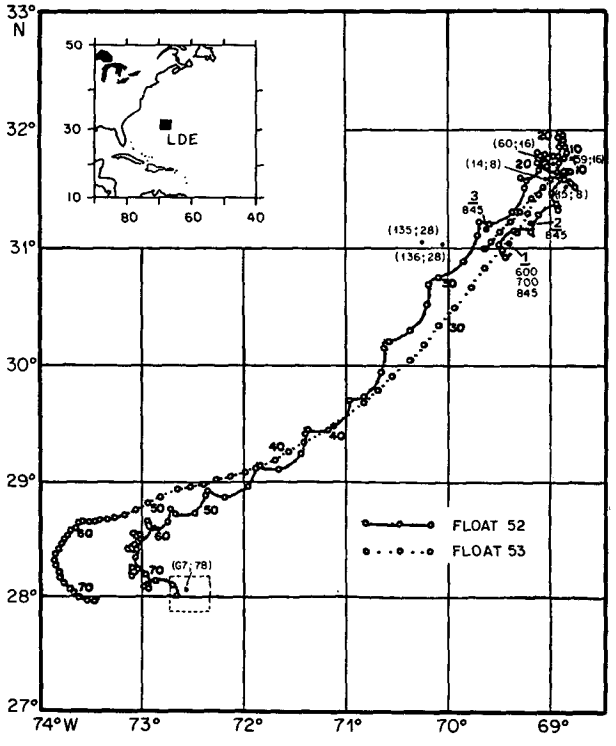

FIG. 1. Trajectories of SOFAR floats 52, at 750 m, and 53, at 700 m. Three fixes per day are plotted for each float, with the first fix given by the open circle. Numbers along the trajectories give the time in days since launch; day 1 is 13 May 1978. Numbers in parentheses along the trajectories denote the numbers and times of hydrographic stations taken in the vicinity of float 52. LDE mooring positions near the float path are given by underlined numbers, with depths of current meters relevant to this study.

a. Horizontal structure

The existence of S1 was first revealed by the trajectories of SOFAR floats 52 and 53, at depths between 750 and 700 m, shown in Fig. 1. Launched 33 km apart in late May of 1978, the floats remained within 73 km of each other through mid-July 1978. During this period, their motion was generally to the southwest at speeds of the order of 20 cm s^{-1}, in accordance with the energetic mesoscale motion present in the LDE region at the time (Shen et al., 1986; Owens et al., 1982). Of particular interest was the cycloidal motion present over the entire trajectory of float 52, but absent from that of float 53, suggesting that float 52 was orbiting a feature having a characteristic horizontal length scale considerably smaller than the 50–100 km horizontal length scale of the energetic mesoscale motions in the region. The orbital period remained constant, between 3 and 4 days, throughout the period of observation. The characteristics of these trajectories are discussed in more detail in Section 3.

Because the floats were tracked in real time [see Spain et al. (1980) for a summary of the tracking procedure], this anomalous motion was observed well before the floats were recovered in late July 1978. Accordingly, an XBT survey of the area around float 52 was made immediately after recovery; a map of the XBT temperatures[2] at 750 m, the depth of float 52, is shown in Fig. 2. The feature S1 appears as the eastward bulge between the 11.3° and 11.5°C isotherms, between XBTs 53 and 62, but is for the most part obscured in this presentation by the slope of the main thermocline at 750 m resulting from the energetic larger scale flow in the vicinity.

b. Vertical structure

In Fig. 3, we show vertical profiles of temperature from XBTs taken approximately along a diameter

[2] The XBTs used in the study, manufactured by Sippican Corporation, were a combination of models T-5 (2000 m depth) and T-7 (850 m depth). It is known that the T-7 type has a systematic temperature error, and temperature profiles from these instruments have been corrected using the calibration curve of McDowell (1977). The T-5 type instruments vary from batch to batch and are more difficult to correct; in this study, corrections were made by calibrating a number of T-5 temperature profiles against simultaneous CTD stations taken during the cruise.

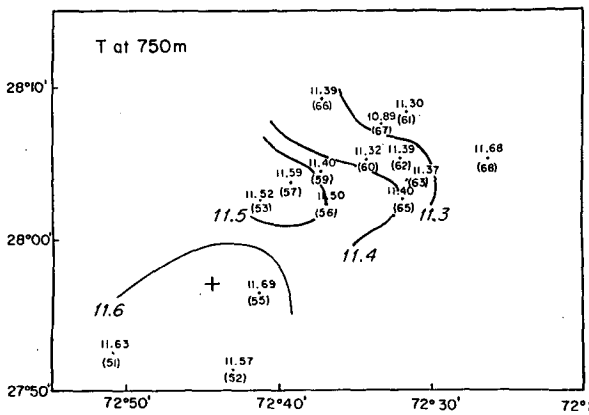

FIG. 2. Temperature (°C) at 750 m as measured during the XBT survey done at the recovery of float 52. Numbers in parentheses are XBT numbers. The cross denotes the recovery position of float 52. Temperatures have been corrected as noted in the text.

through the feature (see Figs. 1 and 2 for station positions). From Fig. 2, we estimate that XBT 59 was closest to the eddy center. Outside the core of the feature, XBTs 55 and 68 are indistinguishable from background Sargasso Sea temperature profiles taken hundreds of kilometers from the center of S1; at a depth of 750 m the vertical temperature gradient computed from these two profiles is 2.5×10^{-3} °C km^{-1}, standard for the western North Atlantic. However, at distances $\leq$ 15 km from XBT 59 the temperature profiles are quite different. Between approximately 11°C and 13°C in each of the profiles lies a region of markedly reduced vertical temperature gradient (a "thermostad"), typically half as large as the background value at XBTs 55 and 68. In each case the thermostad is 150–200 m thick, centered on the 12°C isotherm. In addition, immediately above and below the thermostad region there appears to be in each of the profiles a thin region ~50 m thick where the temperature gradient is somewhat larger than the background. The prominent thermostad evident in Fig. 3 suggests that S1 has a lenslike vertical structure, although the details of the structure are obscured by the larger-scale structure of the temperature field.

In addition to the XBT data taken at the recovery of float 52, CTD station G7 was occupied at the estimated center of the feature immediately following the recovery. Both the salinity and σ_θ profiles from station G7 (shown in Fig. 4) indicate anomalous vertical gradients corresponding to the thermostad region, and the dissolved oxygen has an anomalously intense minimum at the depth of the thermostad.

The temperature/salinity relation at the center of S1, from station G7 (Fig. 5a), appears to be rather standard for the Sargasso Sea when viewed on a scale that encompasses the water from the surface to the bottom of the main thermocline, although there is perhaps a hint of a weak negative salinity anomaly around 11°C, at or slightly below 750 m. When examined as a function of potential density, however (Fig. 5b), the true magnitude of the salinity anomaly at the center of S1 emerges. The maximum anomaly occurs on the σ_θ = 27.05 level; the measured salinity at this potential density, 35.42‰, is more than 5 standard deviations below the mean salinity at this potential density (35.53‰) estimated from over 400 CTD–O_2 stations occupied from 29°–33°N, 67°–71°W during the LDE. Viewed as a function of potential density, the salinity anomaly at the center of S1 appears to be confined roughly between 675 and 800 m. A similar striking anomaly is present in the dissolved O_2 at the center of S1 (Fig. 5c). At σ_θ = 27.05 the measured O_2 value, 2.89 ml l^{-1}, is 5 standard deviations below the ensemble-mean value computed from the entire LDE dataset, 3.74 ml l^{-1}. Again, the strongest part of the anomaly appears to be confined between 675 and 800 m, although the O_2 anomaly appears to be slightly thicker than the salinity anomaly. In an effort to quantify the strength of the pycnostad at the center of S1, we show in Fig. 5d a computed profile of the vortex stretching component of potential vorticity, q, defined as $(f/\rho_0)(\partial\rho/\partial z)$, at the center of S1 from station G7. Here ρ_0 is a reference density, ρ is the potential density, z is a vertical coordinate, and f is the Coriolis parameter. For large-scale ocean flows having weak relative vorticity, we expect that q should be approximately conserved following the motion of a fluid parcel. In this example, where the relative vorticity is clearly not small, there is no need for q alone to be conserved. Nonetheless, q does provide a useful measure of the vertical stratification. At σ_θ = 27.05, the computed value of q at the eddy center, 7.1×10^{-13} cm^{-1} s^{-1}, is 4 standard deviations below the LDE ensemble mean. The region of anomalous q appears to be somewhat thinner than the regions of anomalous salinity and oxygen, probably owing to the larger noise inherent in

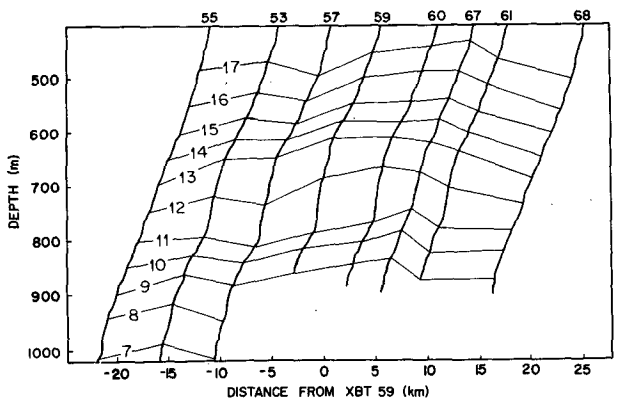

FIG. 3. A collection of XBT traces taken approximately along a diameter through S1. Positions of these traces are shown in Fig. 2. Temperatures have been corrected as described in the text. The distance along the horizontal axis is given by the position of the 12° isotherm.

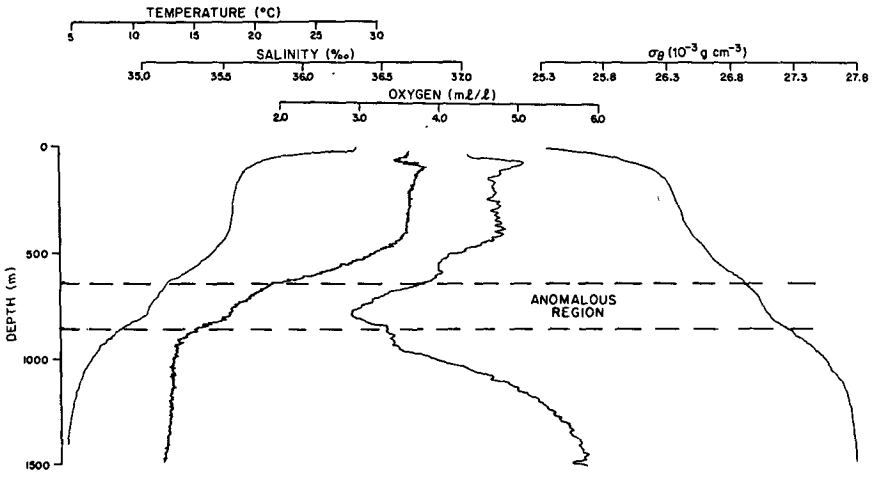

FIG. 4. Profiles of temperature, salinity, dissolved oxygen, and σ_θ from station G7, within 1 km of the center of S1 at 28°04'N, 72°37'W on 27 July 1978 with anomalous region shown. The data were collected using a Plessey Model 9040 CTD with a Beckmann dissolved O_2 sensor. The O_2 values plotted have been smoothed to remove variations on scales shorter than 7.5 m.

estimating q. The gradients have been computed by linear least-square fits to the σ_θ profile over intervals of 50 m, although the computed values of q change little for averaging intervals between 10 and 70 m.

As a final comment on the vertical structure of S1 at its center, we show in Fig. 5e measured values of silicate and nitrate at station G7, as a function of σ_θ. The means and standard deviations on σ_θ surfaces for these variables are taken from Ebbesmeyer et al. (1986), who analyzed nutrient data from some 32 hydrographic stations taken roughly within a 500-km radius of the LDE center a year prior to the LDE. The silicate values at the center of S1 compare favorably with the large-scale mean results. However, the three NO_3 samples closest to the σ_θ = 27.05 surface show large (greater than two standard deviations away from the mean) anomalies, in apparent coincidence with the anomalies of salinity, dissolved oxygen, and vortex stretching discussed above.

As noted previously, a large number of CTD-O_2 stations were occupied on a regular grid during the two month LDE (Taft et al., 1986). Other than at the time of the recovery of float 52, however, no small-scale surveys of S1 were specifically done as part of the LDE hydrographic program. However, a number of CTD casts were fortuitously taken near S1 as it moved through the hydrographic array, and in retrospect these stations can be used to examine the combined horizontal-vertical structure of S1.

Given the trajectory of float 52 (Fig. 1) and making the assumption that the eddy was axially symmetric, the position of the center of S1 can be determined as a function of time between the float launch and recovery; this procedure is described in detail in Section 3 that follows. From a knowledge of the estimated eddy center as a function of time, we have searched the total LDE hydrographic data set for stations near to S1 taken between May and July 1978; a suite of six CTD-O_2 stations each taken within 25 km of the feature's center, plus the station G7, are displayed in Fig. 6 as a function of radius from estimated center, without regard to time. The station locations and dates are shown on Fig. 1.

The large salinity anomaly at the center of S1 on σ_θ = 27.05 (Fig. 6a) appears to be clearly present only in stations G7 and 15 at about 5 km from the eddy center. There are possible remnants to the salinity signal at stations 14, 59 and 136 at 7, 8 and 18 km from the center, though if present at these stations the salinity anomaly is very weak. At radii greater than 18 km from the center (stations 60 and 135) there is no evidence of any salinity anomaly on σ_θ = 27.05. It also appears that a deeper negative salinity anomaly, centered near σ_θ = 27.2 and strongest at station 14, 7 km from the center of S1, is present in several of the profiles; the nature of this feature is unknown.

An alternate view of the vertical-radial structure of S1 is given by the oxygen distribution, shown in Fig. 6b. On σ_θ = 27.05, the large negative O_2 anomaly is evident at radii of 1 and 5 km, and some remnant of the O_2 signal is clearly apparent as far as 8 km from the center.

3. Velocity structure and estimates of dynamical quantities

It is useful to interpret the velocity observations in S1 in terms of a simple model. As was noted above, float 52 appeared to be circling the eddy center with a period of 3–4 days. This suggests fitting a model to the float positions of the form

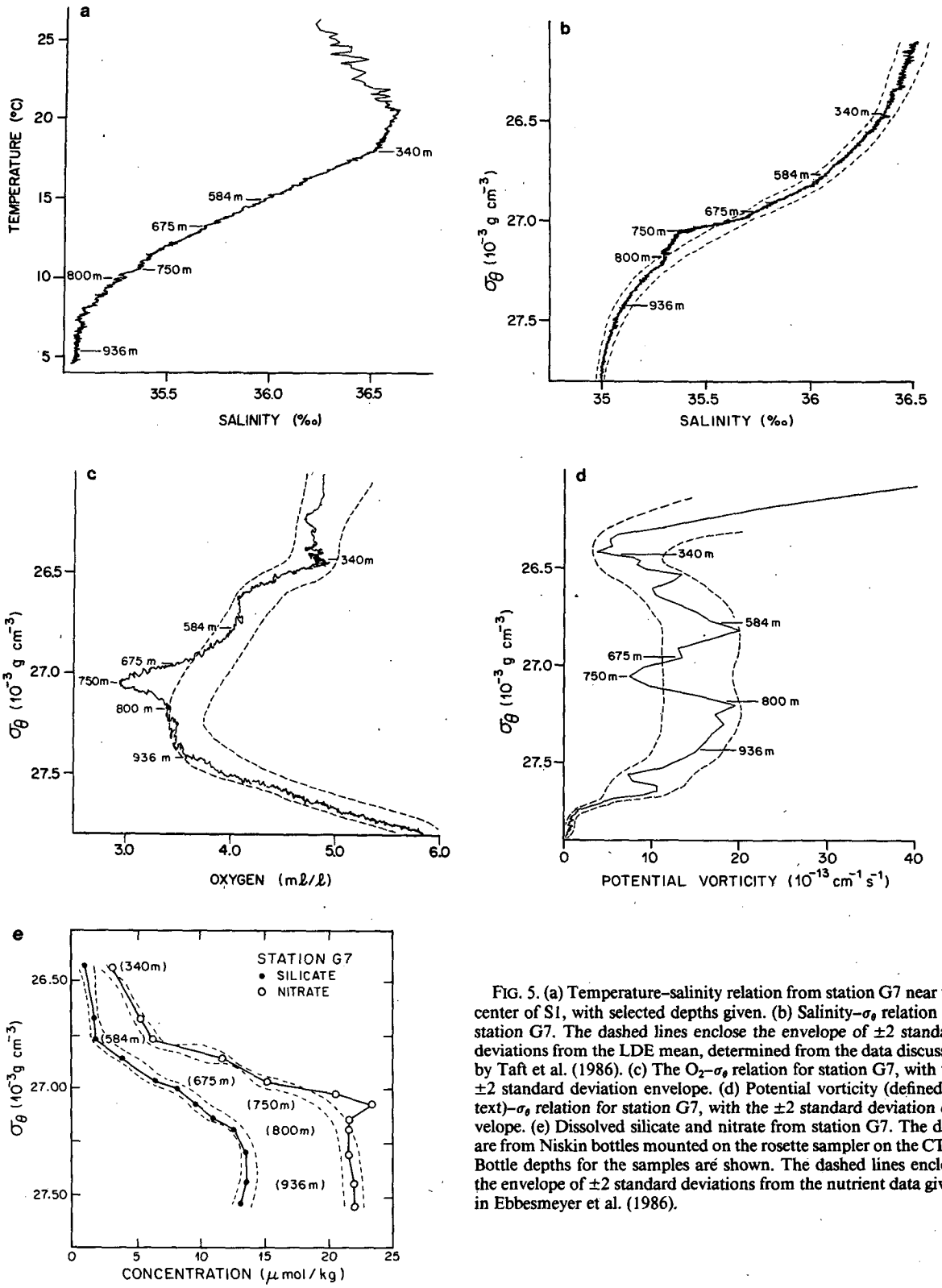

FIG. 5. (a) Temperature–salinity relation from station G7 near the center of S1, with selected depths given. (b) Salinity–σ_θ relation for station G7. The dashed lines enclose the envelope of ±2 standard deviations from the LDE mean, determined from the data discussed by Taft et al. (1986). (c) The O_2–σ_θ relation for station G7, with the ±2 standard deviation envelope. (d) Potential vorticity (defined in text)–σ_θ relation for station G7, with the ±2 standard deviation envelope. (e) Dissolved silicate and nitrate from station G7. The data are from Niskin bottles mounted on the rosette sampler on the CTD. Bottle depths for the samples are shown. The dashed lines enclose the envelope of ±2 standard deviations from the nutrient data given in Ebbesmeyer et al. (1986).

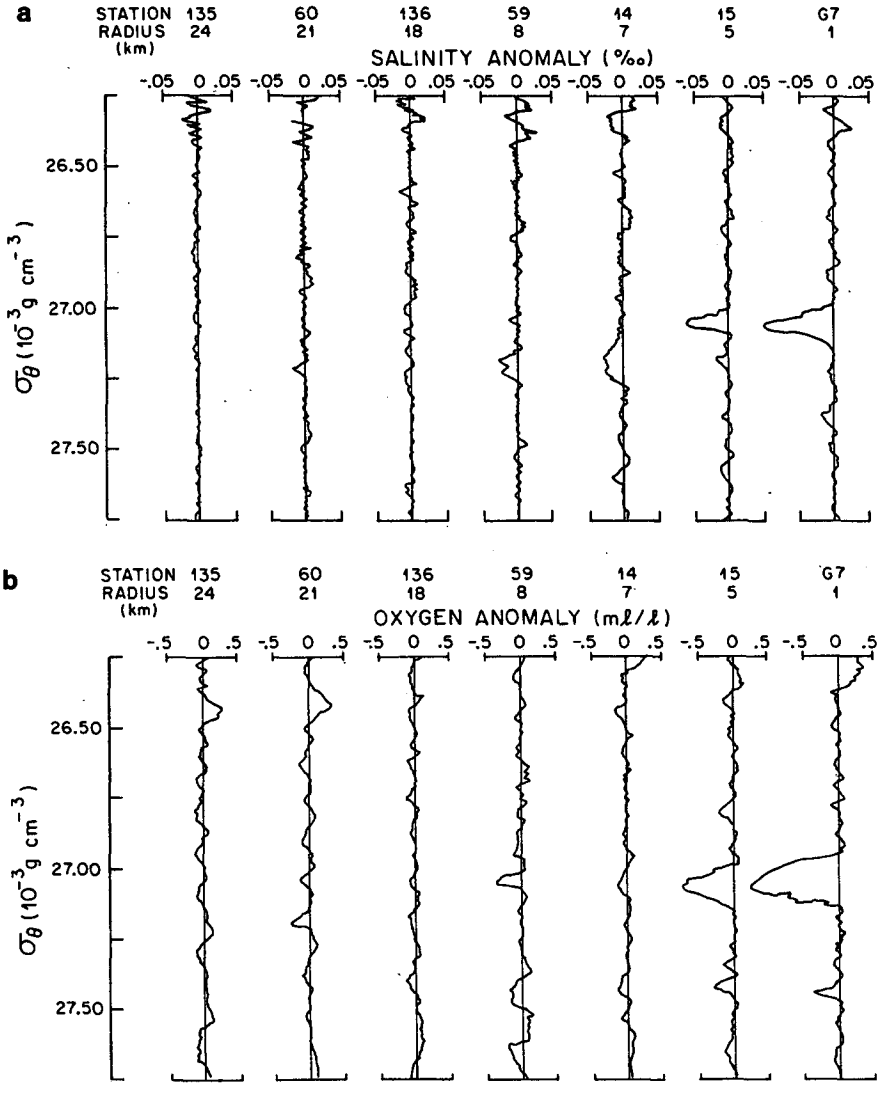

FIG. 6. (a) Salinity anomaly versus σ_θ for a suite of stations taken near S1 from May–July 1978. The station positions are shown in Fig. 1. The estimated radius from the center of S1 is shown, computed as described in the text. The mean salinity for the LDE region, taken from Taft et al. (1986), has been subtracted from the observed values. (b) Dissolved O_2 anomaly versus σ_θ for the same suite of stations. The mean O_2 for the LDE region, taken from Taft et al. (1986), has been subtracted from the observed values.

$$x = x_0 + u_0 t + r\cos(\omega t + \phi_1) \quad (1a)$$

$$y = y_0 + v_0 t + r\sin(\omega t + \phi_1) \quad (1b)$$

where x and y are the eastward and northward displacements from an origin chosen as 31°N, 69°30'W; t is the time from the center of the interval over which the fit is made; and ω is the frequency of rotation of the eddy, chosen as $2\pi/84$ h. The variables of the model were fitted by least squares over an interval of one period (84 h) every half period (42 h) to give a time series of the position of the center of the eddy, (x_0, y_0), the translation velocity of the eddy, (u_0, v_0), the radius of the float orbit, r, and a phase ϕ_1. It should be noted that in this procedure if the frequency of the oscillation shifts to a new frequency, ω_1, then there will be a linearly varying time dependence for the phase,

$$\dot{\phi}_1 = \omega_1 - \omega, \quad (2a)$$

or

$$\phi_1 = (\omega_1 - \omega)t + \phi_0. \quad (2b)$$

A similar fit was also made to the float velocity data with a model of the form

$$u = u_1 + a_x t + v_\theta \sin(\omega t + \phi_2) \quad (3a)$$

$$v = v_1 + a_y t + v_\theta \cos(\omega t + \phi_2) \quad (3b)$$

where the model variables are the translation velocity (u_1, v_1), the acceleration of the eddy, (a_x, a_y), the tangential velocity, v_0, and a phase, ϕ_2. The translation velocities were consistent between the two fits, and the accelerations were quite small.

Shown in Fig. 7 are the fits for the radius of the float orbit, tangential velocity, and the phase for the velocity fit. The radius ranges from 7 to 12 km and the tangential velocity from 13 to 27 cm s^{-1}. The float positions have absolute errors of 2–3 km (Spain et al., 1980) but have relative errors that are considerably smaller, of the order of 0.75 km. The velocities have been calculated from centered differences of the positions and therefore have an error of approximately $\sqrt{2} \cdot (75 \text{ km})/$ 0.667 day or 2 cm s^{-1}. Thus the radius and azimuthal velocities each have errors of about 10%. These errors are the cause of the higher-frequency variations in Fig. 7. The radius and velocity appear to be correlated such that the period for the float to circulate around the eddy, proportional to r/v_0, remains more nearly constant than either of the two variables r and v_0. The plot of the phase for the velocity shows that the float's orbital period remains within 8 hours of the assumed value of 84 hours.

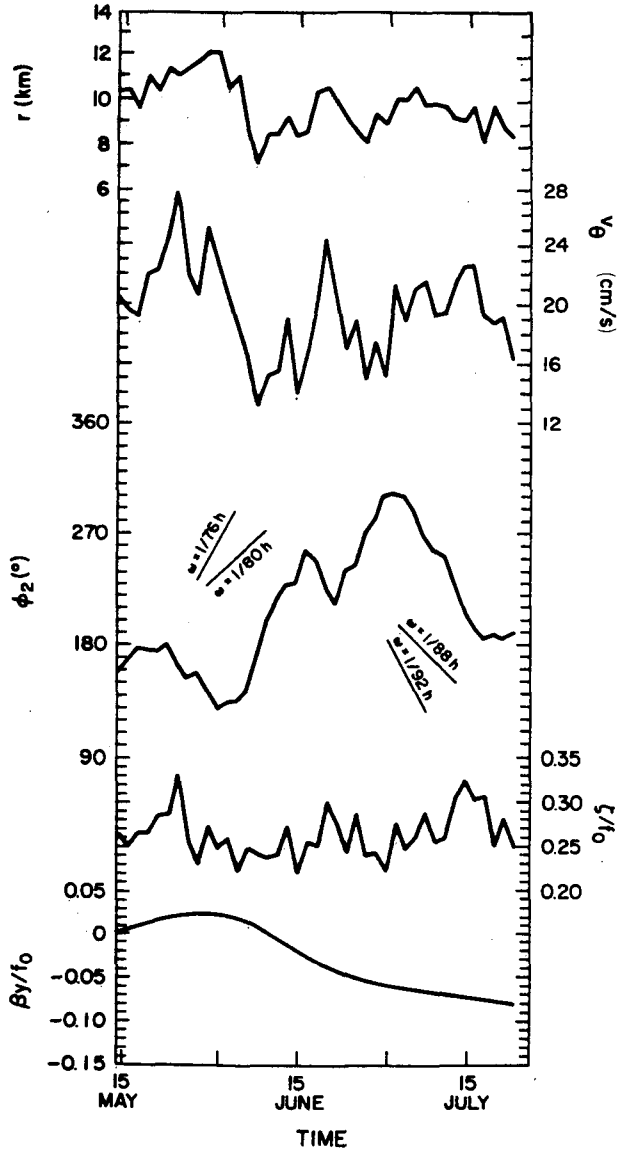

FIG. 7. The radius r of float 52; v_θ; ϕ_2; ζ/f_0; and $\beta y/f_0$ as a function of time, computed as described in the text.

As noted, the eddy moved near to several LDE moorings during the period from May to August 1978 (see Fig. 1). It is possible to investigate the spatial structure of S1 using the moored current meters to display the measured velocities in a reference frame moving with the eddy. Assuming the eddy to be moving at a constant translation velocity, estimated from the float data for the interval when the eddy passed a mooring, the current meters will appear to make a straight section through the eddy. The results of this approach are shown in Fig. 8 for the LDE central mooring. The current meters were vector-averaging current meters (VACMs) with a 15-minute sampling rate. A running Gaussian filter with an 8-hour half-width was applied to the data and the resulting time series was subsampled at 8-hour intervals to reduce as much of the smaller-scale (internal wave and tidal) variability as possible without smearing out the eddy signal. The current meter data have been discussed in detail by Owens et al. (1982).

The eddy passed very close to the central mooring of the LDE current meter array. This mooring was heavily instrumented in the vertical so that the vertical extent of the velocity signal could be determined. At depths of 500 m and above, and 2000 m and below, there was no appreciable signal associated with the eddy. The results for 600 m depth have been included in Fig. 8 although the eddy signal is not readily discernible above the noise associated with the small-scale variability that would obscure any signal below 4–5 cm s^{-1}. The results at 600 m depth for other moorings are noisy and have not been shown. At 700 m depth the largest velocity signal can be seen. Also shown in Fig. 8 is the azimuthal velocity as a function of radius, determined before and after the float passed the mooring. A maximum velocity of 20 cm s^{-1} occurs at a radius of 10–12 km. The structure of the velocity suggests that the streamfunction (or pressure) field of the eddy can be modeled (see Fig. 9) as

$$\psi = \psi_0 \exp\left\{-\left[\frac{r^2}{\gamma^2} + \frac{(z - z_0)^2}{\delta^2}\right]\right\} = \psi_0 \exp(-\Omega)$$

which gives a geostrophic velocity structure of the form

$$v_0 = -\frac{\psi_0}{\gamma^2} r \exp(-\Omega)$$

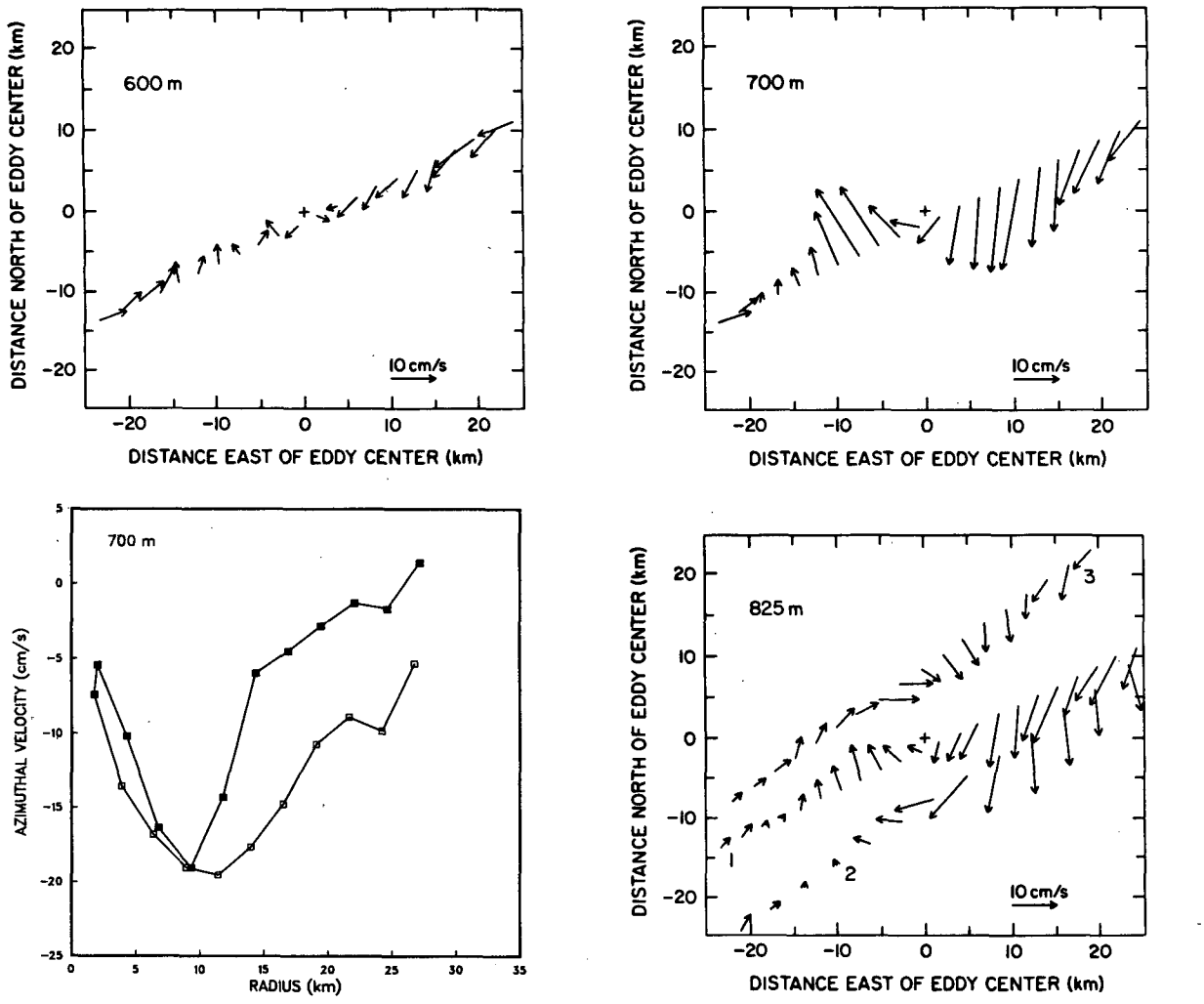

FIG. 8. (a) The velocity vector at 600 m on the central mooring (number 1) as S1 passed the mooring. The east and north distances are measured from the eddy center to the mooring. (b) As for (a), but at 700 m on the central mooring. (c) Azimuthal velocity at 700 m as a function of radius from the eddy center, determined from the central mooring. Solid (open) points are computed from the time when the eddy was east (west) of the mooring. (d) As for (a), but at 825 m on the central mooring, and also for moorings 2 and 3.

with a maximum tangential velocity at $r = \pm\sqrt{\gamma/2}$ and $z = z_0$. This model of the spatial structure has been chosen because it is differentiable and gives an azimuthal velocity and vertical displacement that are also continuous. It should be noted that this model is not a unique descriptor of the eddy structure and can probably not be distinguished statistically from other simpler models. It should, therefore, only be considered as a tool to combine and compare the horizontal- and vertical-scale estimates obtained from the velocity and temperature data.

At 825 m the eddy signal is evident both at the central mooring (number 1) and at moorings northeast (number 2) and northwest (number 3) of the central mooring. These moorings sampled the eddy as it moved northeast from the central mooring and later after it had reversed its direction and moved towards the southwest. For the central mooring, the velocity maximum occurs at the same distance from the eddy center as seen at 700 m depth, but with a magnitude reduced to 12 cm s^{-1} at 825 m. The apparent pattern and magnitude seen at the other moorings are similar to those for the central mooring.

As was the case for the hydrographic and XBT data taken when float 52 was recovered, the moored velocity data suggests a short vertical scale for the eddy. If we take values of the swirl velocity at 600, 700 and 825 m depth of 4, 20 and 12 cm s^{-1} (where the first value is an uncertain upper limit), then the Gaussian streamfunction model would give a vertical half-width of 100 m and a maximum swirl velocity of 23 cm s^{-1} at 740 m depth. This is consistent with the tangential velocity estimated from float 52 (Fig. 7), which was at a nominal depth of 750 m (Spain et al., 1980). The Gaussian

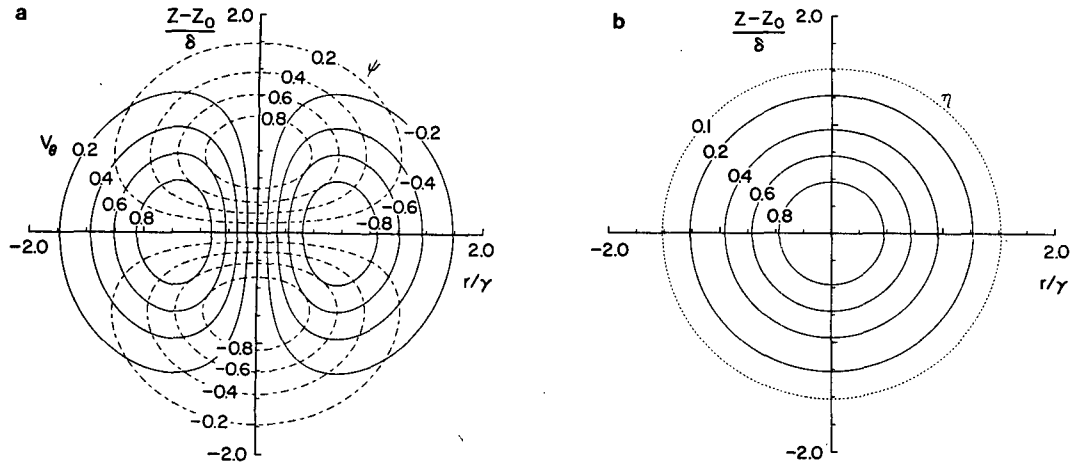

FIG. 9. (a) ψ and v_θ normalized by their maximum values for an eddy of the form $\psi = v_0 \exp(-\Omega)$, assuming quasi-geostrophic balance. (b) η normalized by its maximum value for such an eddy.

model would predict an isopycnal displacement of the form

$$\eta = -\frac{f\psi_0}{N^2}\frac{(z - z_0)}{\delta^2}\exp(-\Omega),$$

which has a maximum absolute displacement at $r = 0$ and $z = z_0 \pm \delta/\sqrt{2}$. Taking $\delta = 100$ m from the velocity fit predicts maximum isotherm displacements 70 m above and below 740 m depth, which is consistent with the observed displacements. The isotherm displacements have a larger vertical scale than the velocity while the velocity has a larger apparent horizontal scale. For example, the isotherm displacements are 20% of their maximum values at 1.75δ, while the velocity is reduced in amplitude by 20% at 1.3δ. The qualitative aspects of this model are consistent with the observed temperature and velocity structure. Although the pattern is consistent with the suggested model, there is one noticeable discrepancy. At all depths and locations there appears to be an asymmetry, with larger velocities to the northeast, especially at large radial distances from the eddy center. This can be explained by the presence of a significant horizontal shear associated with the larger-scale flow.

The Rossby number associated with this eddy, $V_0/(fr)$, where V_0 is the maximum of v_θ, is approximately 0.25. Although the Rossby number is certainly not infinitesimally small, we expect that the eddy's dynamics can be approximately cast in terms of the conservation of quasi-geostrophic potential vorticity (Pedlosky, 1979). In a reference frame moving with the eddy, potential vorticity should be conserved. That is,

$$\zeta + \frac{f_0 h}{H} + \beta y = \text{constant},$$

where ζ is relative vorticity, $\hat{\mathbf{z}} \cdot \nabla \times \mathbf{u}$; h is the change in thickness between two isopycnals from the mean thickness, H; and the Coriolis parameter is $f = f_0 + \beta y$, where βy is the variation in planetary vorticity.

Using the time series of the tangential velocity and radius of the float orbit calculated from the float trajectory, an estimate of the relative vorticity for the eddy can be made. As we have seen from the moored velocity data, the float is trapped in the eddy at the radius of maximum velocity. Assuming the eddy to be axially symmetric, the relative vorticity

$$\zeta = \hat{\mathbf{z}} \cdot \nabla \times \mathbf{u} = \frac{v_\theta}{r} + \frac{\partial v_\theta}{\partial r} - \frac{1}{r}\frac{\partial v_r}{\partial \theta}$$

reduces to

$$\zeta = \frac{v_\theta}{r}$$

at the location of the float. Shown in Fig. 7 is the time series of relative vorticity, at float 52, scaled by the planetary vorticity at 31°N, f_0. Although there are large changes with periods of 20–30 days in both the tangential velocity and the radius, they tend to compensate so as to keep the relative vorticity constant. Thus, relative vorticity for the eddy can be considered to be constant during the period of observation. The higher-frequency variations are due to noise in the float position and velocity fits over 84 hours. Also plotted in Fig. 7 is the change in planetary vorticity, evaluated at 31°N, where y is the distance north of that latitude. This curve has also been normalized by f_0. Clearly, relative vorticity is not changing to compensate for the changes in planetary vorticity.

Taking the temperature measurements at the central mooring and the depths of the 11° and 13°C isotherms for both the XBT survey after the float was recovered and for the two times, 22 and 29 May 1978 (when CTD stations made as part of the larger-scale LDE hydrographic survey were taken in and near the eddy) estimates of the vortex stretching can be made. The

TABLE 1.

Station	Distance from eddy center	Date (1978)	Depths of isotherms 13°C	11°C	h/H
LDE Mean			693	781	
Central Mooring (Temperatures are at 615 and 840 m)					
Before eddy	25		15.22	10.26	−0.03
		12 May	14.01	10.04	0.54
After eddy	25		14.73	9.77	−0.005
Large-Scale Surveys					
Gyre 16			700	795	0.07
Gyre 15	5	22 May	679	820	0.59
Gyre 14			669	777	0.22
Gyre 58			721	823	0.15
Gyre 59	8	29 May	699	847	0.67
Gyre 60			693	806	0.28
XBT Survey after Float 52 recovery					
XBT 55	17		691	796	0.19
53	11		640	783	0.62
57	5		647	811	0.85
59	0	28 July	632	803	0.93
60	5		635	791	0.76
67	8		638	778	0.55
61	12		663	802	0.57
68	20		674	768	0.06

moored temperature measurements have been converted to equivalent displacements of isotherms using

$$\eta = (T - \bar{T}) \frac{\partial \bar{T}}{\partial z}$$

where the overbar indicates mean quantities averaged over all the LDE data as compiled by Taft et al. (1986). The 11° and 13°C isotherms have been chosen since they are close to the depth of maximum vertical displacements.

The estimates of vortex stretching are given in Table 1. The entries have been ordered so that observations are given from west to east for each time the eddy was sampled. When the eddy was moving northward, during the large-scale surveys, the isotherms sloped upwards to the west indicating a northward baroclinic velocity (assuming a deep reference level). During the XBT survey when the eddy was moving southward, the slope had reversed and was consistent with a southward baroclinic velocity. The estimates of the thickness from the moored temperatures are an underestimate of the actual vertical displacements, since the actual changes in the thickness are larger than the simple linear temperature/displacement conversion assumed above will allow.

Comparing samples at similar distance from the eddy center, we cannot detect any systematic changes in thickness that are above the scatter seen in the individual observations within each survey. The 8% change in thickness necessary to compensate for the change in planetary vorticity is somewhat less than the noise level inherent in this analysis, and thus we cannot with confidence discern a measurable change in the vortex stretching over the course of the experiment that might balance the change in planetary vorticity.

4. Origin scenarios

Given the chemical and physical properties discussed in the preceding sections, we examine the question of

FIG. 10. (a) Pressure (db) of the $\sigma_\theta = 27.0$ surface in the North Atlantic, from McDowell et al. (1982). (b) Salinity (‰) on the $\sigma_\theta = 27.05$ surface for the North Atlantic, from McDowell (1982). (c) Dissolved oxygen (ml l^{-1}) on the $\sigma_\theta = 27.05$ surface for the North Atlantic, from McDowell (1982). (d) Potential vorticity (10^{-13} cm^{-1} s^{-1}) between the $\sigma_\theta = 27.0$ and 27.3 surfaces, from McDowell et al. (1982). In each of these figures the data used were from the IGY dataset (Fuglister, 1960); for (a)–(c) the data were linearly interpolated to the surface of interest. The $\sigma_\theta = 27.00$ surface is within 20 m of the $\sigma_\theta = 27.05$ surface over most of the North Atlantic. The LDE region is shown as a box.

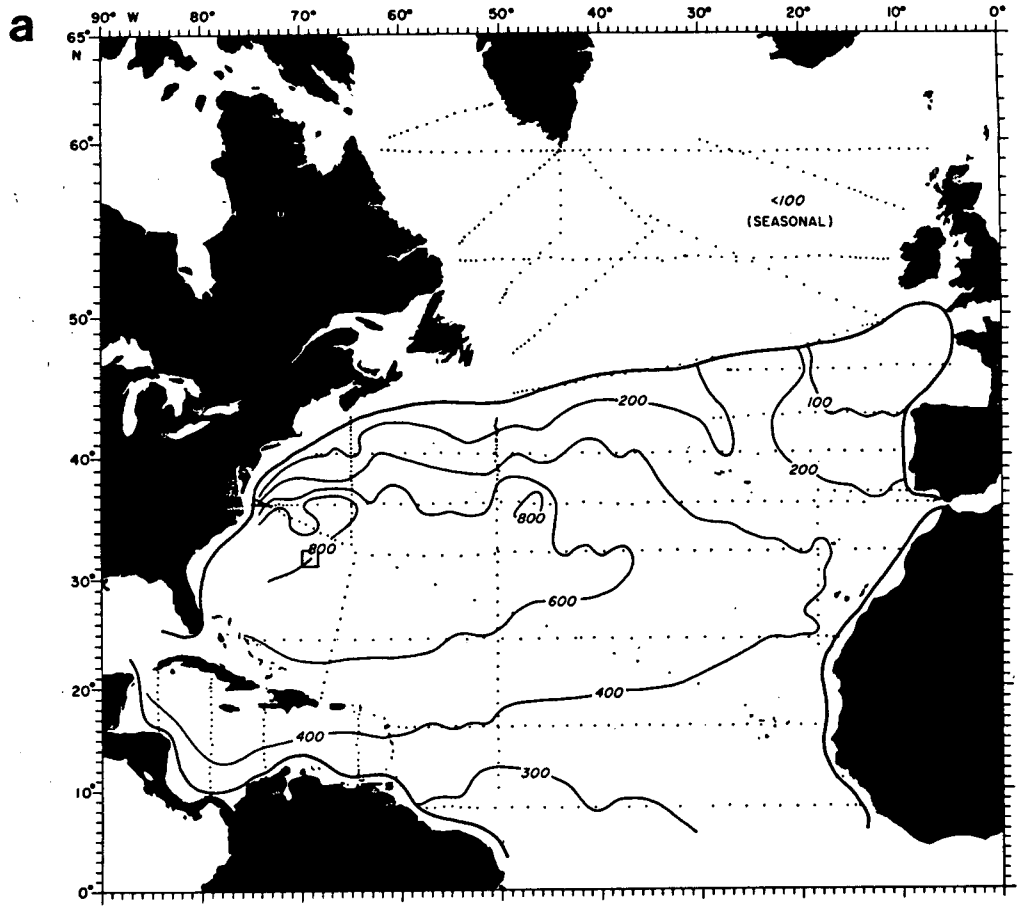
a
90° W
80°
70°
60°
50°
40°
30°
20°
10°
0°
65° N
60°
50°
40°
30°
20°
10°
0°
<100
(SEASONAL)
200
100
200
800
800
600
400
400
300

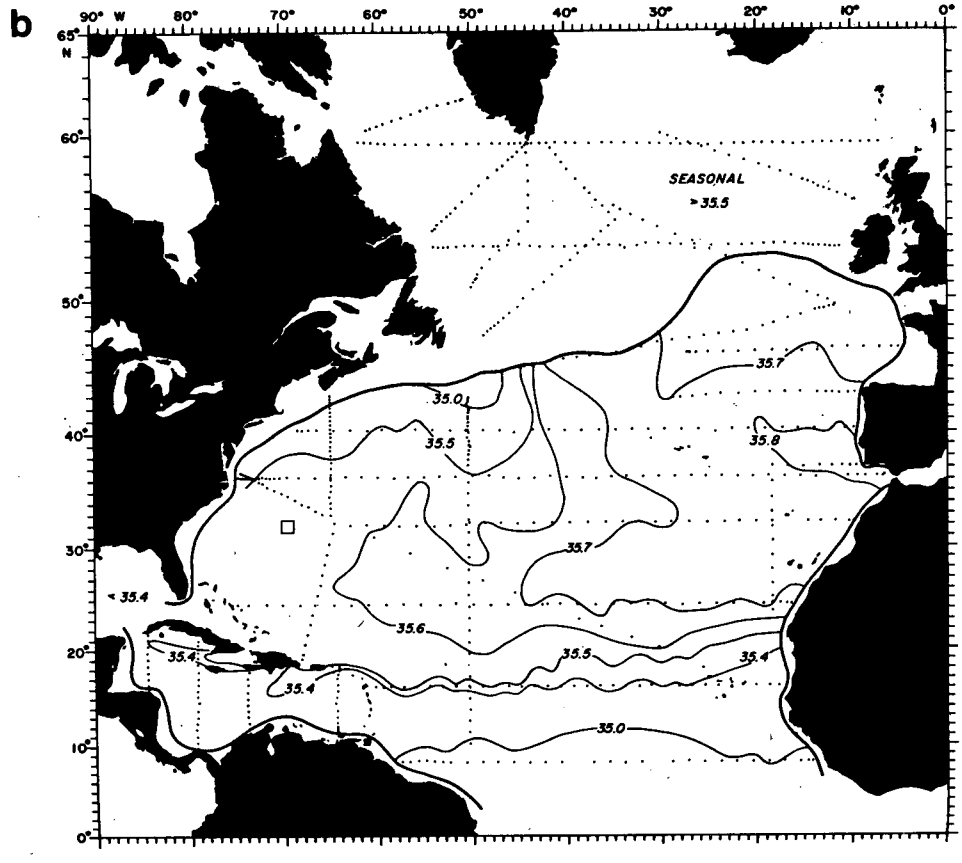
b
90° W
80°
70°
60°
50°
40°
30°
20°
10°
0°
65° N
60°
50°
40°
30°
20°
10°
0°
SEASONAL
> 35.5
35.7
35.0
35.5
35.8
35.7
< 35.4
35.6
35.4
35.5
35.4
35.4
35.0

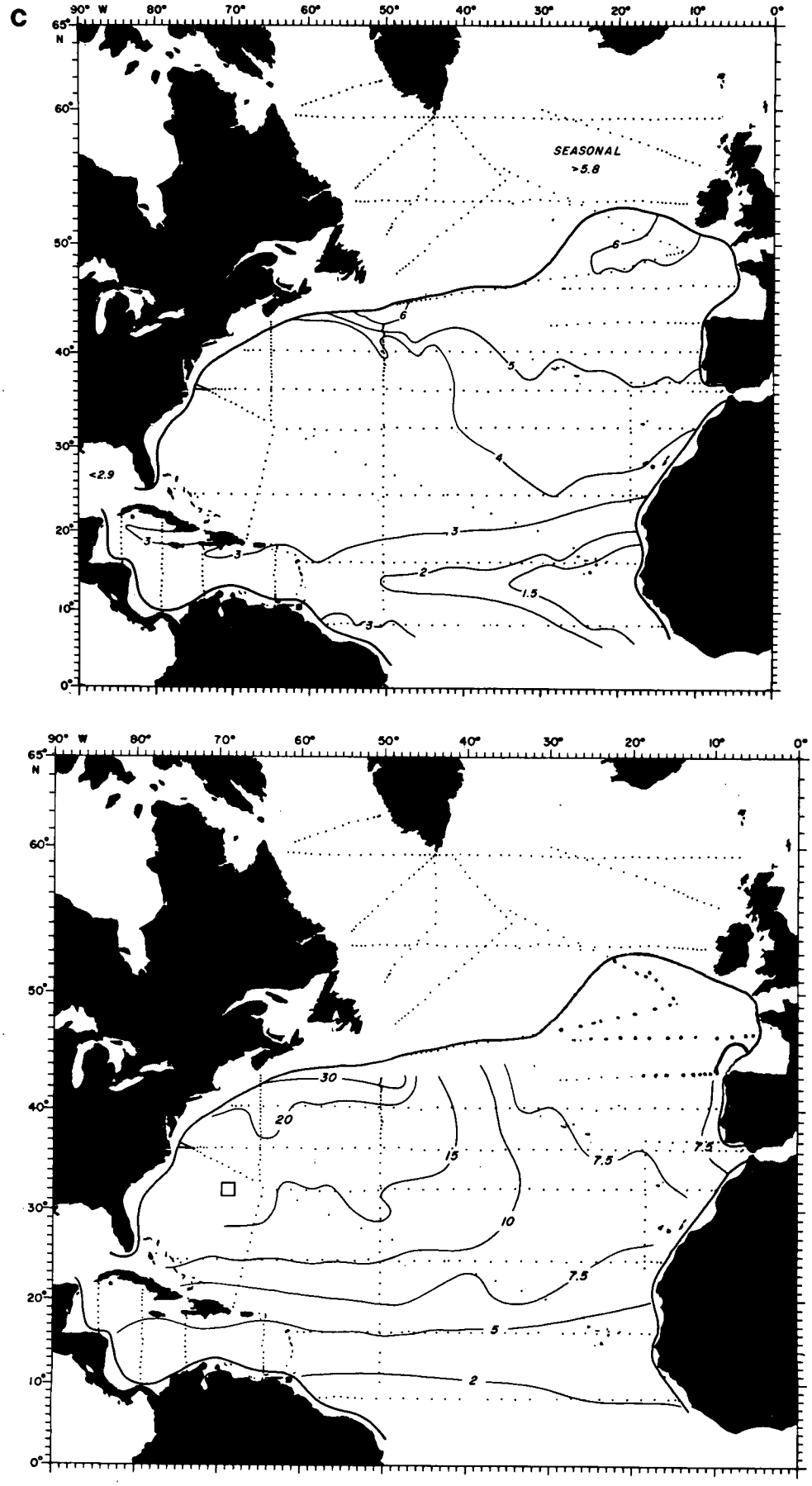
c
d
90° W
80°
70°
60°
50°
40°
30°
20°
10°
0°
65° N
60°
50°
40°
30°
20°
10°
0°
SEASONAL
>5.8
6
6
5
4
1
<2.9
3
3
3
3
2
1.5
3
30
20
15
7.5
7.5
10
1
7.5
5
2

the origin of S1. Clearly this question is not a simple one, as we have only indirect and fragmentary evidence concerning the feature's history. We shall begin by examining the anomalous properties of the feature in the context of the large-scale North Atlantic circulation. In Fig. 10, we show contour plots of salinity and dissolved O_2 (taken from McDowell, 1982) on the $\sigma_\theta = 27.05$ surface for the North Atlantic, and vortex stretching, q, computed between the 27.0 and 27.3σ_θ surfaces (taken from McDowell et al., 1982). In each case the data used were taken from the International Geophysical Year dataset (Fuglister, 1960). The data consisted of Nansen bottle casts, and the S and O_2 values shown in Fig. 10 have been linearly interpolated to the $\sigma_\theta = 27.05$ surface. It is clear from these diagrams that the thermocline shoals towards the eastern boundary of the basin at this level and that a recirculating gyre is present in the western basin. In addition, the highest salinity values on this density level originate in the Mediterranean outflow at the eastern boundary, and there is a region of relatively high salinity extending across the basin, bounded both on the north and south by lower salinity regimes. The highest O_2 values occur in the northern part of the basin, where the surface outcrops in the winter, while the lowest occur in the southeast corner and extend to the west in a tongue from the coast of Africa.

At the core of S1 we have, on $\sigma_\theta = 27.05$, observed the following values:

$$\left.\begin{aligned} S &= 35.42‰ \\ O_2 &= 2.89 \text{ ml l}^{-1} \\ q &= 7.1 \times 10^{-13} \text{ cm}^{-1} \text{ s}^{-1} \end{aligned}\right\}.$$

From Fig. 10, it is seen that these values are not typical of the large-scale ambient characteristics of the LDE region, the vicinity of 31°N, 60°30'W. It appears that water possessing these particular large-scale characteristics is found on the $\sigma_\theta = 27.05$ surface *only south of approximately 20°N*. Thus, assuming that the primary mode of mixing is along potential density surfaces, it is likely that water of the type in S1 originated a minimum of one thousand kilometers away from where it was observed. There is no lack of water with the desired properties, however. South of 20°N, virtually the entire North Atlantic has water with characteristics similar to those observed in S1.

While Fig. 10 gives some indication where water with the observed characteristics might be found in the North Atlantic and indicates that the water in S1 is anomalous for the LDE region, it is also necessary to take into account mixing and nonconservative effects between the source of the water and the point of observation. For example, the observed O_2 value in the core of S1, 2.9 ml l^{-1} on $\sigma_\theta = 27.05$, could have decreased from a once higher value at the point of origin; Jenkins (1982) has estimated the O_2 consumption in the North Atlantic to be ~0.06 ml l^{-1}/yr in the vicinity of $\sigma_\theta = 27$. The dissolved O_2 in S_1 could have also possibly changed through mixing. In addition, given the large negative salinity anomaly in the feature on $\sigma_\theta = 27.05$, it is possible that the salinity was once even lower than the observed value and was raised by mixing between the points of origin and observation.

To investigate further the possible origins of S1, we examine a number of the variables measured in S1, as a function of salinity on the $\sigma_\theta = 27.05$ surface. We have compared our S, O_2 and q estimates for S1, along with the dissolved NO_3 and silica samples collected, with the North Atlantic GEOSECS data (Bainbridge, 1981). The North Atlantic GEOSECS stations were taken along essentially two sections (Fig. 11), one paralleling the Mid-Atlantic Ridge from pole to equator, and one from the eastern to western boundary between 22° and 38°N. In Fig. 12, we show various properties from the GEOSECS dataset, linearly interpolated to the $\sigma_\theta = 27.05$ surface, as a function of the measured salinity linearly interpolated to that surface, and similar properties from the S1 observations. In all cases the bottle spacing was 102 m or less vertically.

While it is impossible to infer an unambiguous origin for S1 from Fig. 12, by comparing the measured S1 properties to the GEOSECS data some consistent patterns do emerge, and we note here the results of this comparison for each of the measured variables.

a. Dissolved O_2

The GEOSECS data indicate a tendency towards an increase in both S and O_2 between the equator and 40°N. North of 40°N the O_2 continues to increase. North of 50°N the $\sigma_\theta = 27.05$ surface outcrops during the winter, and the O_2 and S observed are highly variable. The higher S values for stations between 20° and 40°N reflect the influence of Mediterranean water, although this potential density surface is somewhat higher in the water column than is usually associated with waters of Mediterranean origin.

The S and O_2 values observed in S1 fall closest to the values for GEOSECS station 36, near 15°N, 54°W. Such a semitropical origin is consistent with the origin inferred from the IGY data (Fig. 10). GEOSECS station 37, slightly to the south of 35, has similar S and O_2 values on this potential density surface, as does (somewhat surprisingly) GEOSECS 121, near 34°N, 68°W. However, we suspect that GEOSECS 121 is itself highly anomalous for the western North Atlantic at $\sigma_\theta = 27.05$. We have found in the National Oceanographic Data Center archives 182 high-quality hydrographic stations (as judged by the criteria given by Ebbesmeyer and Taft, 1979) in the region 32°–36°N, 66°–70°W; the mean salinity on $\sigma_\theta = 27.05$ from this ensemble was 35.54‰, with a standard deviation of 0.07‰. If the salinity is normally distributed around its mean value, then we would expect that only 14% of the possible

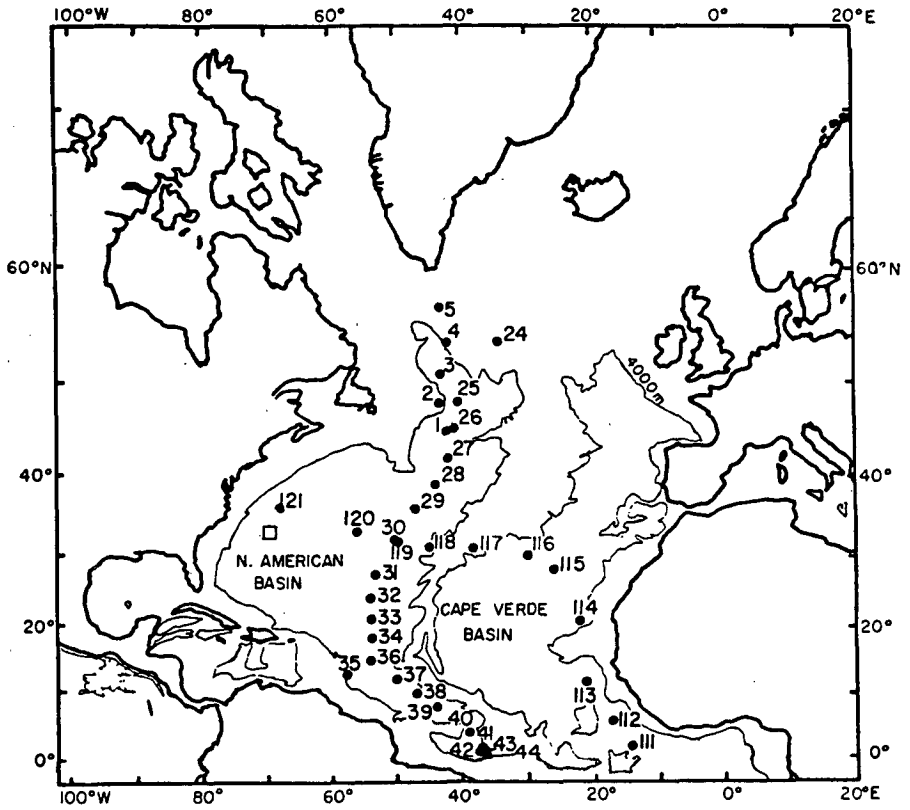

FIG. 11. Positions and numbers of the GEOSECS stations taken in the North Atlantic used in the computations in this study. The boxed region denotes the LDE area.

salinity values in this region would be below 35.44‰, the interpolated value of salinity on $\sigma_\theta = 27.05$ from GEOSECS station 121. The O_2 values on $\sigma_\theta = 27.05$ at GEOSECS station 121 appear to be even more anomalous than the salinity. Using the dissolved O_2 data from eight stations taken between 33°N and 37°N along 68°30'W during the Gulf Stream '60 experiment (Fuglister, 1963), we compute a mean dissolved O_2 on $\sigma_\theta = 27.05$ of 3.61 ml l^{-1}, with a standard deviation of 0.09 ml l^{-1}. Again assuming a normal distribution, we would expect that fewer than 1% of the possible O_2 values in this region would be less than 3.27 ml l^{-1}, the interpolated value of O_2 on $\sigma_\theta = 27.05$. The appearance of such an anomaly, similar to S1 in chemical properties, suggests that such small-scale anomalies may not be as rare in the western North Atlantic as simple statistical inferences from Gaussian distributions would suggest.

b. *Dissolved* NO_3

The NO_3 values shown in Fig. 12 reflect a general increase towards the equator south of 50°N. This complements the O_2 variability previously discussed: as the O_2 is consumed biologically the NO_3 increases, as do other nutrients. As with O_2, NO_3 is not a conservative tracer of water masses but can reflect qualitative characteristics. The measured salinity and NO_3 in S1 were, on $\sigma_\theta = 27.05$, closest to the values at GEOSECS station 36, with GEOSECS stations 37 and 121 having similar properties. Again, GEOSECS 121 would appear to be somewhat out of place on the diagram.

c. "NO"

This is a composite property, equal to $9NO_3 + O_2$ for each station in Fig. 11; the O_2 values shown in Fig. 12 have been multiplied by a factor of 43.48 in order

FIG. 12. (a) Dissolved O_2 as a function of salinity on the $\sigma_\theta = 27.05$ surface, using data from GEOSECS stations shown in Fig. 11. Both O_2 and S values have been linearly interpolated to the $\sigma_\theta = 27.05$ surface. Numbers on the plot refer to GEOSECS station numbers. The asterisk denotes the measured values at station G7, at the center of S1. The stippled region encloses an ensemble of values for the Gulf of Mexico, computed by linearly interpolating the hydrographic data of Morrison and Nowlin (1977) onto the $\sigma_\theta = 27.05$ surface. The mean values for the LDE region, determined from the data of Taft et al. (1986) and Ebbesmeyer et al. (1986), are shown by the symbol ⊙. (b) As in (a), but for dissolved nitrate. (c) As in (a), but for "NO" (Broecker, 1974). (d) As in (a), but for dissolved silicate. (e) As in (a), but for potential vorticity, computed as discussed in the text.

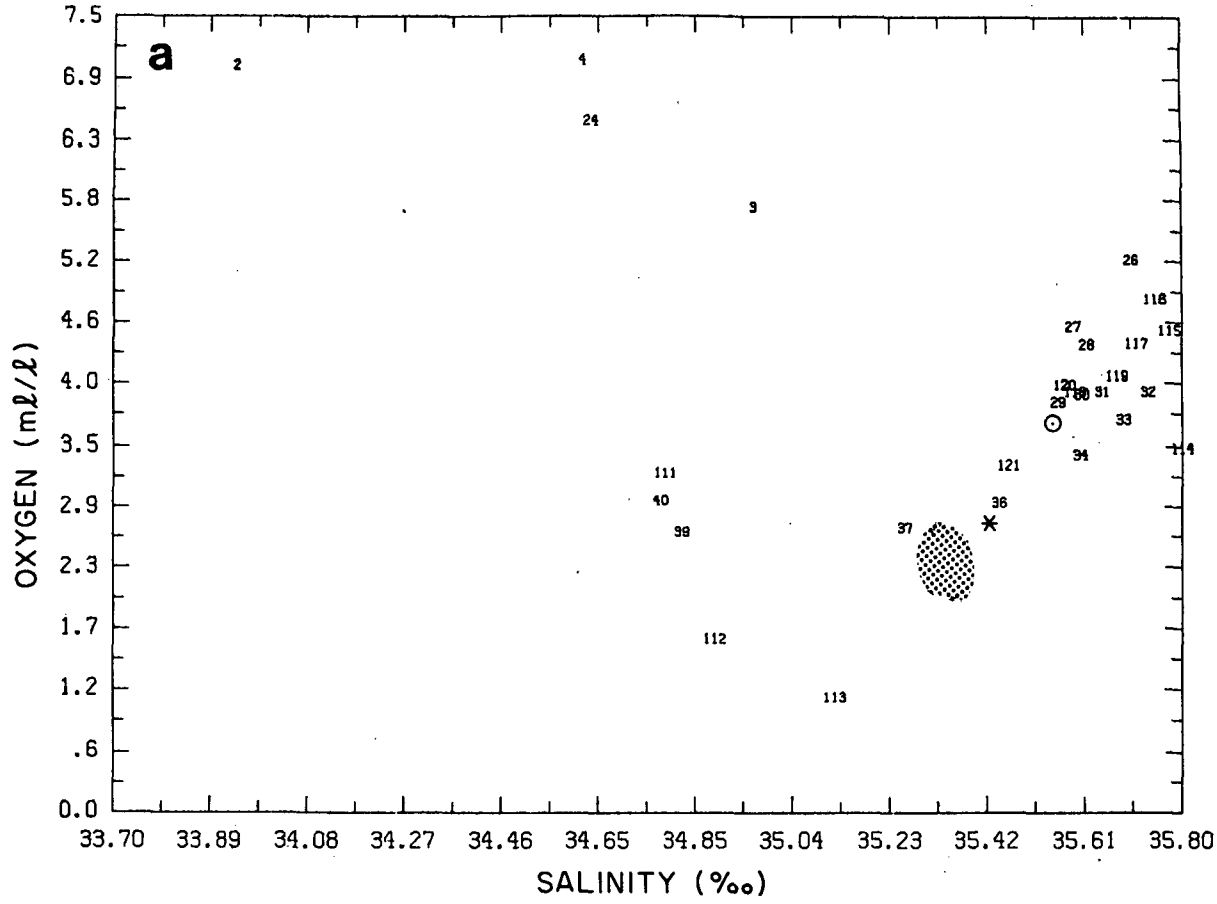
a
OXYGEN (mℓ/ℓ)
7.5
6.9
6.3
5.8
5.2
4.6
4.0
3.5
2.9
2.3
1.7
1.2
.6
0.0
33.70
33.89
34.08
34.27
34.46
34.65
34.85
35.04
35.23
35.42
35.61
35.80
SALINITY (‰)

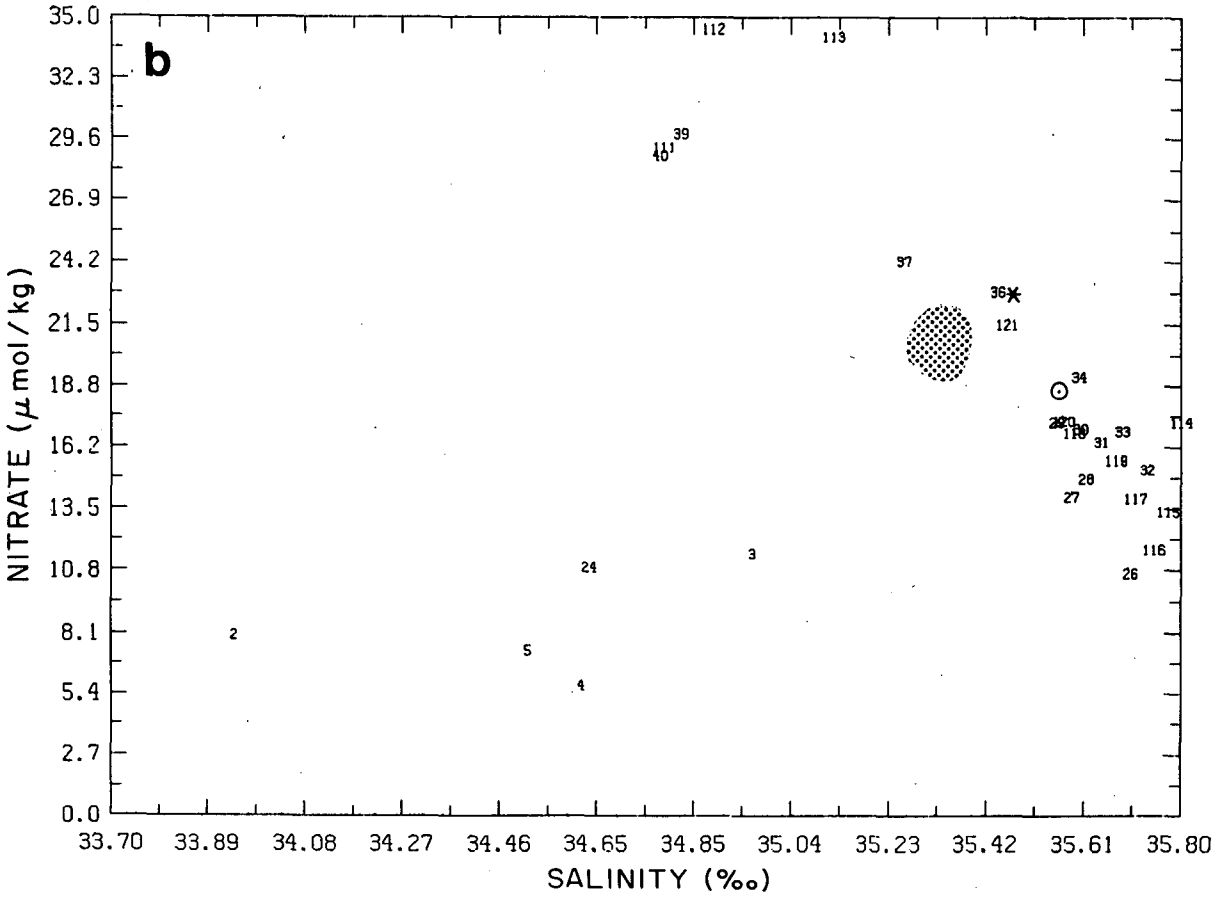
b
NITRATE (μmol/kg)
35.0
32.3
29.6
26.9
24.2
21.5
18.8
16.2
13.5
10.8
8.1
5.4
2.7
0.0
33.70
33.89
34.08
34.27
34.46
34.65
34.85
35.04
35.23
35.42
35.61
35.80
SALINITY (‰)

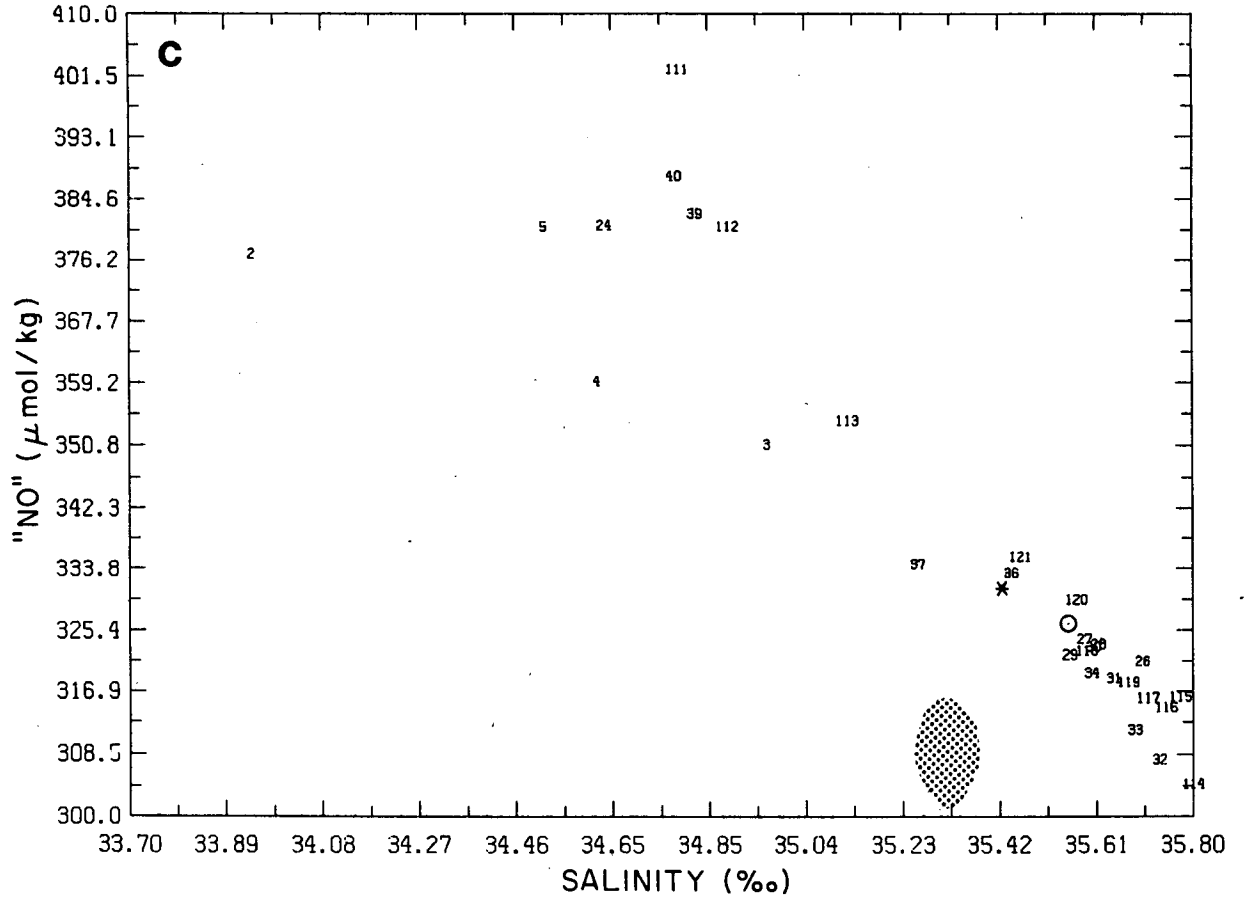
c
"NO" (μmol/kg)
410.0
401.5
393.1
384.6
376.2
367.7
359.2
350.8
342.3
333.8
325.4
316.9
308.5
300.0
33.70
33.89
34.08
34.27
34.46
34.65
34.85
35.04
35.23
35.42
35.61
35.80
SALINITY (‰)

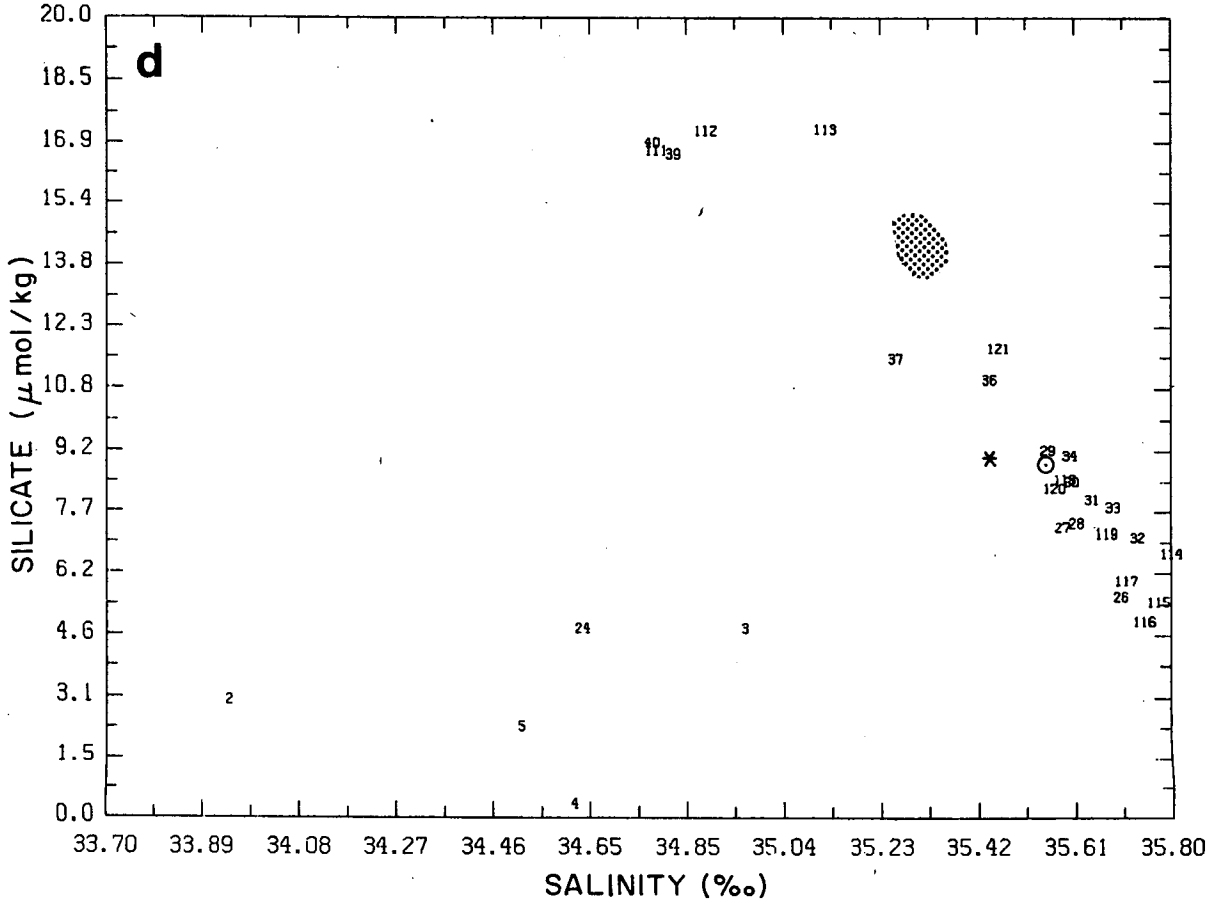
d
SILICATE (μmol/kg)
20.0
18.5
16.9
15.4
13.8
12.3
10.8
9.2
7.7
6.2
4.6
3.1
1.5
0.0
33.70
33.89
34.08
34.27
34.46
34.65
34.85
35.04
35.23
35.42
35.61
35.80
SALINITY (‰)

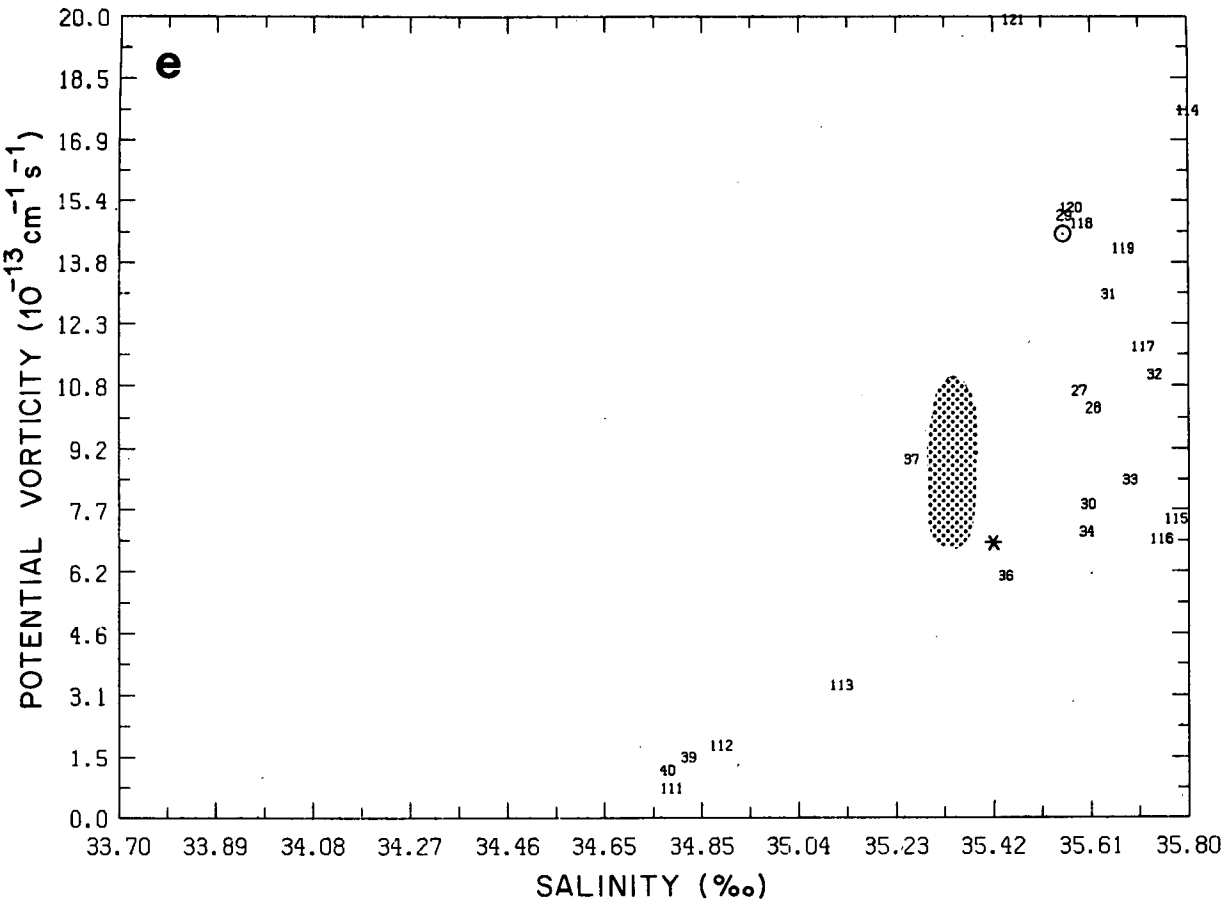

FIG. 12. (*Continued*)

to convert them to units of μmol kg^{-1} before making the computation. The use of "NO" was suggested by Broecker (1974), who noted that, while neither NO_3 nor O_2 were conservative themselves, "NO" should be conservative as long as the classical model of biological breakdown suggested by Redfield (1942) was operative. We see in Fig. 12 relatively high values of "NO" near the equatorial and polar regions, with a "NO" minimum at midlatitudes. As Broecker (1974) has shown, this distribution is related to meridional variations in biological productivity and circulation. The measured "NO"-salinity values in S1 on $\sigma_\theta = 27.05$ are, as with O_2 and NO_3, closest to the values from GEOSECS stations 36 and 121.

d. *Dissolved silicate*

Dissolved silicate is lowest near the eastern boundary at midlatitudes, at the highest salinities, corresponding to water of Mediterranean origin. The lowest dissolved silica values are, generally, in polar and equatorial regions. The silicate value from S1 on $\sigma_\theta = 27.05$, 7.7 μmol kg^{-1}, paired with the corresponding salinity, falls nearest GEOSECS stations 29, 34, 36 and 120, although it does not fall directly on any of these stations. From the measured silicate on $\sigma_\theta = 27.05$ in S1, it does not appear to be possible to discern a unique origin for the feature.

e. *Vortex stretching*

The vortex stretching component of potential vorticity, q, is a maximum at midlatitudes near the western boundary, reflecting the westwardly recirculating wind gyre (Worthington, 1976). The high q values near the western boundary are a measure of the large amount of warm water present there, resulting in a relatively deep thermocline. Here S1 appears to have nearly the same q and salinity on $\sigma_\theta = 27.05$ as GEOSECS station 36; while other stations have similar values of q, only GEOSECS 37 has a salinity within 0.1‰ of that observed in S1. We note again, however, that strictly speaking, q should only be conserved following a fluid parcel for the large-scale mean circulation, and the apparent agreement with the origin inferred from other properties may be fortuitous. The q values plotted in Fig. 12 were computed by fitting a quadratic function to the potential density samples nearest the $\sigma_\theta = 27.05$ surface (two points above and one below) and then evaluating the vertical derivative at the depth of the

$\sigma_\theta = 27.05$ surface. This procedure resulted in a marked reduction in the scatter of q values in Fig. 12 compared with evaluation of q by linear interpolation.

It thus appears that GEOSECS station 36, near 15°N, 54°W, provides the closest match to the properties observed in S1, on $\sigma_\theta = 27.05$, suggesting an origin for the water in the feature nearly 2000 km from where it was observed. In such a case the parent water mass for S1 would consist of a mixture of Antarctic Intermediate Water moving north along the coast of South America (as discussed by Montgomery, 1938), and the large pool of Tropical Atlantic Central Water (discussed by Sverdrup et al., 1942) existing in the equatorial Atlantic, resulting from a mixture of North and South Atlantic Central Waters. This does, in fact, seem to be a plausible explanation for the origin of the feature. Montgomery (1938) showed that large water property gradients exist on isopycnal surfaces near $\sigma_\theta = 27.05$ in this region, and Mazeika (1973) from dynamic computations and Fu et al. (1982) from moored current meters have shown that relatively energetic eddies and mean flows are present there. Thus it is not inconceivable that the local dynamical variability, coupled with large water property gradients, could occasionally result in isolated lenses, in much the same fashion that Gulf Stream rings are generated at higher latitudes in the basin. A boundary current flowing northwest along the Antilles island arc, if existent, could then carry such features into the greater LDE region. However, the existence of such an Antilles Current has long been controversial, and recent work (Olson et al., 1984) suggests that such a current does not exist in an Eulerian mean sense. This does not preclude the occasional northward transport of subtropical water along the island arc, however.

While the region near 15°N, 54°W represents one location where the feature could have originated, it is by no means the only one; the Gulf of Mexico also appears to be a plausible source. To illustrate this, in Fig. 12 we have included data from the ensemble of stations discussed by Morrison and Nowlin (1977), taken in the eastern Gulf of Mexico. As with the GEOSECS data, the bottle data from the Gulf has been interpolated to the $\sigma_\theta = 27.05$ surface. On this σ_θ surface the maximum salinity from the ensemble is slightly below that in S1. On the other hand, the ensemble of O_2, NO_3 and q values presented in Fig. 12 for the Gulf are as near to the values observed in S1 as any GEOSECS station other than number 36.

That the water in the eastern Gulf of Mexico is similar to the water off the Lesser Antilles is not unexpected. A number of investigators (Wüst, 1964; Metcalf, 1976) have shown that water on the Atlantic side of the Antilles enters the Caribbean through various passages and exits through the Yucatan Strait into the Gulf of Mexico. Some of this water eventually passes through the Florida Straits and back into the North Atlantic via the Gulf Stream, possibly then to be recirculated through the LDE area. In fact, a water mass having similar values of temperature, salinity, and vortex stretching near the $\sigma_\theta = 27$ surface to those observed in S1 has been shown to exist at a depth near 500 m in the Florida Straits by Brooks and Niiler (1977). Moreover, an early paper by Seiwell (1937) suggested the presence of a tongue of water of low dissolved O_2 penetrating from the Gulf of Mexico through the Florida Straits, apparently disappearing near Cape Hatteras. Thus, while it seems likely that the water in S1 acquired its characteristics thousands of kilometers south of the LDE region, it is possible that the eddy itself was formed much closer to the point of observation. This then suggests a second scenario for the origin of S1 that, based on the data shown in Fig. 12, seems as plausible as an origin near GEOSECS station 36.

Other, quite different, origin scenarios are possible, and indeed, seem not unlikely. In examining the GEOSECS data presented in Fig. 12, for example, it is clear that a water type similar to that of S1 can be formed by mixing water from GEOSECS stations 113 and 115; this is consistent for each of the measured variables. The previous two scenarios suggest an origin for S1 at or near the western boundary of the North Atlantic; yet stations 113 and 115 are at the eastern boundary, in a region of large meridional property gradients, and it is reasonable that at some latitude between them a water type similar to that found at the core of S1 exists.

Thus, overall, while we cannot discern a unique origin for S1 from the available data, we can suggest several reasonable origin scenarios that are not inconsistent with the observations. Most importantly, it appears likely that the water type in the feature S1 originated in a region far removed from the LDE area.

5. Summary and discussion

We have described here in detail the characteristics of one small-scale feature observed in the main thermocline of the western North Atlantic during the LDE. Yet, even given the relatively detailed observations presented here, a number of first-order questions concerning S1 and other similar features remain unanswered. We do not know, for example, how common such features are in the ocean. The LDE small-scale eddy census of Lindstrom and Taft (1986) suggests that such features may exist throughout the water column in the LDE region and may occur not infrequently. On the other hand, we have little knowledge of the likelihood of finding such features in other parts of the world's oceans. Thus an appraisal of the importance of such features in large-scale ocean mixing, perhaps the most crucial issue raised by these observations, cannot be given at the present time. In addition, we know essentially nothing of how such features are formed. While we have assumed here that, between the source of such features and the point of observation, mixing takes place only along isopycnal surfaces, other

mixing scenarios, such as near-surface convective overturning, may be possible that yield identical water types. Once such features have formed, we have little notion as to how they move about. The SOFAR float observations (Fig. 1) suggest that S1 was passively advected by the larger-scale background flow around it. However, theoretical arguments (Killworth, 1983) suggest that such features could be self-advected under some circumstances.

It seems clear that, given the large property anomalies associated with S1, the property fluxes resulting from an ensemble of similar features could potentially be a substantial fraction of the total property fluxes in a basin, if such features are not uncommon. An accurate assessment of this question will require both a better knowledge of the space–time distribution in the ocean of small-scale features such as S1 and a better knowledge of the mean properties of the world's oceans, so that both the origin of such features and their property fluxes in relation to the mean circulation can be better discerned.

Acknowledgments. We are thankful to our numerous LDE colleagues for discussions concerning these ideas over the past several years. We are particularly grateful to Eric Lindstrom for providing the material shown in Fig. 6. This work was supported by the National Science Foundation by grants OCE-82-14541 and OCE-84-16537 (SR) and OCE 79-01087 (Bruce Taft) to the University of Washington, and grants OCE 77-19403 (WBO) to Woods Hole Oceanographic Institution and OCE 78-18662-A02 (HTR) to the University of Rhode Island.

REFERENCES

Bainbridge, A. E., 1981: GEOSECS Atlantic Expedition. Vol. 1, Hydrographic Data. National Science Foundation.

Brooks, I. H., and P. P. Niiler, 1977: Energetics of the Florida Current. *J. Mar. Res.*, **35,** 163–191.

Broecker, W. S., 1974: "NO", a conservative water mass tracer. *Earth Planet. Sci. Lett.*, **23,** 100–107.

Ebbesmeyer, C. C., and B. A. Taft, 1979: Variability of potential energy, dynamic height, and salinity in the main pycnocline of the western North Atlantic. *J. Phys. Oceanogr.*, **9,** 1073–1089.

——, ——, J. C. McWilliams, C. Y. Shen, S. C. Riser, H. T. Rossby, P. E. Biscaye and H. G. Ostlund, 1986: Detection structure, and origin of extreme anomalies in a western Atlantic Oceanographic section. *J. Phys. Oceanogr.*, **16,** 591–612.

Elliott, B. A., and T. B. Sanford, 1986: The subthermocline lens D1. Part I: Description of its density structure, water properties, and velocity profiles. *J. Phys. Oceanogr.*, **16,** 532–548.

Fu, L. L., T. Keffer, P. P. Niiler and C. Wunsch, 1982: Observations of mesoscale eddy variability in the western North Atlantic: A comparative study. *J. Mar. Res.*, **38,** 533–569.

Fuglister, F. C., 1960: *Atlantic Ocean Atlas of Temperature and Salinity Profiles and Data from the International Geophysical Year of 1957–58.* WHOI Atlas Ser. Vol. 1, 209 pp.

——, 1963: Gulf Stream '60. *Progress in Oceanography,* Vol. 1, Pergamon, 265–373.

Jenkins, W. J., 1982: On the climate of the subtropical ocean gyre: Decade timescale variations in water mass renewal in the Sargasso Sea. *J. Mar. Res.*, **40**(Suppl.), 265–290.

Killworth, P. D., 1983: On the motion of isolated lenses on a Betaplane. *J. Phys. Oceanogr.*, **13,** 368–376.

Lindstrom, E. J., and B. A. Taft, 1986: Small water-property transporting eddies: Statistical outliers in the hydrographic data of the POLYMODE Local Dynamics Experiment. *J. Phys. Oceanogr.*, **16,** 613–631.

Mazeika, P. A., 1973: Circulation and water masses east of the Lesser Antilles. *Dtsch. Hydrogr. Z.*, **26,** 49–73.

McDowell, S. E., 1977: A Note on XBT accuracy. POLYMODE News, 29, WHOI, Unpublished Manuscript.

——, 1982: Analyses of North Atlantic Intermediate Waters along isopycnal surfaces and within mesoscale eddies. Ph.D. thesis, University of Rhode Island.

——, P. Rhines and T. Keffer, 1982: North Atlantic Potential Vorticity and its Relation to the General Circulation. *J. Phys. Oceanogr.*, **12,** 1417–1436.

——, and H. T. Rossby, 1978: Mediterranean water: An intense mesoscale eddy off the Bahamas. *Science,* **202,** 1085–1087.

Metcalf, W. G., 1976: Caribbean-Atlantic water exchange through the Anegada-Jungfern Passage. *J. Geophys. Res.*, **81,** 6410–6409.

Montgomery, R. B., 1938: Circulation in the upper layers of the southern North Atlantic deduced with use of isentropic analysis. *Pap. Phys. Oceanogr. Meteorol.*, **6,** 1–55.

Morrison, J. M., and W. D. Nowlin, Jr., 1977: Repeated nutrient, oxygen, and density sections through the loop current. *J. Mar. Res.*, **35,** 105–128.

Olson, D., F. Schott, K. Leaman and R. Zantopp, 1984: The mean circulation east of the Bahamas as determined from a recent measurement program and historical XBT data. *J. Phys. Oceanogr.*, **14,** 1470–1487.

Owens, W. B., J. R. Luyten, and H. L. Bryden, 1982: Moored velocity measurements on the edge of the Gulf Stream recirculation. *J. Mar. Res.*, **40**(Suppl.), 509–524.

Pedlosky, J., 1979: *Geophysical Fluid Dynamics.* Springer-Verlag, 624 pp.

Redfield, A. C., 1942: The processes determining the concentration of oxygen, phosphate, and other organic derivatives within the depths of the Atlantic Ocean. *Pap. Phys. Oceanogr. Meteorol.*, **9,** 5–22.

Rossby, H. T., J. Price and D. Webb, 1986: The spatial and temporal evolution of a cluster of SOFAR floats in the POLYMODE Local Dynamics Experiment (LDE). *J. Phys. Oceanogr.*, **16,** 428–442.

Seiwell, H. R., 1937: The minimum oxygen concentration in the western basin of the North Atlantic. *Pap. Phys. Oceanogr. Meteorol.*, **5,** Number 3.

Shen, C. Y., J. C. McWilliams, B. A. Taft, C. C. Ebbesmeyer and E. J. Lindstrom, 1986: The mesoscale spatial structure and the evolution of dynamical and scalar properties during the POLYMODE Local Dynamics Experiment. *J. Phys. Oceanogr.*, **16,** 454–482.

Spain, D. L., R. M. O'Gara and H. T. Rossby, 1980: SOFAR float data report of the POLYMODE Local Dynamics Experiment. University of Rhode Island Graduate School of Oceanography, Tech. Rep. 80-1.

Sverdrup, H. U., M. W. Johnson and R. H. Fleming, 1942: *The Oceans.* Prentice-Hall, 1087 pp.

Taft, B. A., E. J. Lindstrom, C. C. Ebbesmeyer, C. Y. Shen and J. C. McWilliams, 1986: Water mass structure during the POLYMODE Local Dynamics Experiment. *J. Phys. Oceanogr.*, **16,** 403–426.

Worthington, L. V., 1976: On the North Atlantic circulation. *Johns Hopkins Oceanographic Studies,* Vol. 6, 110 pp.

Wüst, G., 1964: *Stratification and Circulation in the Antillean-Caribbean Basins.* Columbia University Press, 201 pp.